Journal of Photochemistry & Photobiology, A: Chemistry 412 (2021) 113249

Contents lists available at ScienceDirect

Journal of Photochemistry & Photobiology, A: Chemistry

journal homepage: www.elsevier.com/locate/jphotochem

Commercial herbicide degradation by solar corrosion Fenton processes of iron filaments in a continuous flow reactor and its computational fluid dynamics (CFD) simulation

Luis A. Castillo-Suárez [a], Ivonne Linares-Hernández [a,*], Ruben Vasquez-Medrano [b], Jorge G. Ibanez [b], Fortunata Santoyo-Tepole [c], Boris Miguel López-Rebollar [a], Verónica Martínez-Miranda [a]

[a] Instituto Interamericano de Tecnología y Ciencias del Agua (IITCA), Universidad Autónoma del Estado de México, Km 14.5 Carretera Toluca-Atlacomulco, C.P. 50200, Toluca, Estado de México, Mexico
[b] Universidad Iberoamericana, Prolongación Paseo de la Reforma 880, Col. Lomas de Santa Fe, Del. Álvaro Obregón, C. P. 01219, Ciudad de México, Mexico
[c] Escuela Nacional de Ciencias Biológicas, Instituto Politécnico Nacional (ENCB-IPN), Prolongación de Carpio y Plan de Ayala s/n, Miguel Hidalgo, Santo Tomás, C.P. 11340, Ciudad de México, Mexico

ARTICLE INFO

Keywords:
Advanced oxidation processes (AOPs)
Corrosion
Paraquat
Gramoxone
Solar Fenton

ABSTRACT

Commercial solutions of paraquat (PQ) herbicide were treated by solar corrosion Fenton processes (SCF). A borosilicate reactor was packed with a coiled filament of annealed iron wire to different reactor volume/filament surface area ratios (V_t/A_f). A cylindrical parabolic concentrator was designed to concentrate UV light. The response surface methodology was used to determine the optimal process conditions using a Box-Behnken design in the removal of PQ, COD, and TOC. The independent variables used in this study were: H_2O_2 concentration (500, 1500, and 2500 mg L^{-1}), hydraulic retention time (HRT) (20, 30, and 40 min), and V_t/A_f (3:1, 6:1 and 9:1 cm^3: cm^2). Solution pH was adjusted to 2.8. The optimal conditions for the removal of PQ were: 2248.7 mg L^{-1} of H_2O_2, an HTR of 28 min, and V_t/A_f of 3.4:1. These yielded a 99.9 % removal of PQ, 100 % removal of COD, and 96.7 % of TOC. Toxicity was 100 % removed with 700 mg L^{-1} of H_2O_2. CFD indicated operating fluid velocity and turbulence contributed to maintaining an adequate Fe^{2+}.

1. Introduction

Paraquat dichloride (PQ) is extremely toxic to humans and animals. It is used in agriculture as an herbicide that induces oxidative stress in cells; its neurotoxicity likely arises from a balance in the redox state of affected cells [1]. The United States Environmental Protection Agency (EPA) and the Environmental Risk Management Authority (ERMA) of New Zealand describe paraquat as toxic chemical for humans, plants, and animals [2,3], and it is also very ecotoxic to aquatic systems [4]. It is widely used in more than 130 countries [1,5]. Farmers apply PQ at a concentration of up to 0.5 % per hectare, depending on the type of crop according to the manufacturer's specifications [5,6]. Concerns about long-term exposures are related to its possible accumulation in the food chain [7]. It has been found to cause hepatotoxicity in *Cyprinus carpio L.* (common carp) at concentrations between 1.5–3.2 mg L^{-1} [8]. PQ accumulates in lungs at up to 6–10 times its plasma concentration, causing damage to the respiratory system [1].

Removal of pollutants from agroindustry wastewaters is a priority [9]. Conventional chemical and biological treatments are not sufficiently effective [8–10] because it is not biodegradable by microorganisms and is considerably recalcitrant [11–13].

Recently, the isolation of microorganisms from the rhizosphere of soils with a history of PQ application has been proposed. These organisms adapted to particular conditions, were isolated and achieved removals between 70 % and 86 % of a 100 mg L^{-1} solution [14]. Removal efficiencies of 54.2 %, 54.1 % and 70.7 % of a 100 mg L^{-1} solution were obtained by the microorganism with 12 days of treatment under controlled conditions of pH, temperature and concentration of nutrients [15]. Microbial remediation is the process of transforming highly toxic compounds into low-toxic or non-toxic products after a series of domestication, enrichment, screening and culturing of the strains; however, these could not produce ideal effects under field conditions

* Corresponding author.
E-mail address: ilinaresh@uaemex.mx (I. Linares-Hernández).

https://doi.org/10.1016/j.jphotochem.2021.113249
Received 6 August 2020; Received in revised form 17 January 2021; Accepted 2 March 2021
Available online 6 March 2021

[14].

Other non-biological mechanisms such as magnetic nanosorbents biopolymers to increase PQ adsorption [16], degradation by photocatalysis using carbon nitride that removes 70 % in 10 h of treatment at an initial concentration of 10 ppm of reactive PQ [17], have been evaluated.

Advanced oxidation processes (AOPs) are effective in the degradation of organic pollutants [6,10]. For example, some authors report that after 3 h, there is 4% and 91 % removal of TOC through photolysis and photocatalysis respectively [15]. Applying electrochemical processes, 79 % yields have been obtained after 1.5 h of treatment using Pt/steel electrodes [16].

Other methods such as photocatalysis with ZrO_2/TiO_2 have obtained 84 % removal with 240 min of radiation [17], and TiO_2 nanostructures with 84.4 % removal in a 5 h of treatment, respectively [18]. Electro-Fenton and photoelectro-Fenton, anodic oxidation, and classic Fenton methods show 94 %, 97 %, 64 % and 51 % COD removal, respectively, for the degradation of PQ [19]. However, there are long reaction times (i.e., 50–400 min), while the current intensity applied in the electro-Fenton process was 400 mA. Although the removal efficiency is high, some processes require a prolonged reaction time, which results in higher electrical energy consumption. This can be related to the characteristic of the structure of the PQ, which is highly persistent [13].

Fenton processes have been widely used in the degradation of persistent organic compounds such as drugs and herbicides, improving biodegradability and reducing the toxicity of the treated effluent [7,14,15]. The main reactions are (Eq.1–6) [20–23]:

$$Fe^{2+} + H_2O_2 \rightarrow Fe^{3+} + \cdot OH + OH^- \quad (1)$$

$$OrgH + \cdot OH \rightarrow Org^{\cdot} + H^{\cdot} + \cdot OH \rightarrow CO_2 + H_2O + ions \quad (2)$$

$$\cdot OH + H_2O_2 \rightarrow HO_2 + H_2O \quad (3)$$

$$Fe^{2+} + \cdot OH \rightarrow Fe^{3+} + OH^- \quad (4)$$

$$Fe^{3+} + HO_2 \rightarrow Fe^{2+} + O_2 + H^+ \quad (5)$$

$$\cdot OH + \cdot OH \rightarrow H_2O_2 \quad (6)$$

Photo-Fenton and solar-Fenton processes improve the removal efficiency of pollutants due to the photoreduction of Fe^{3+} to Fe^{2+}, which increases the generation of the hydroxyl radical following Eq. 7 [16,17]:

$$Fe^{3+} + H_2O + hv \rightarrow Fe^{2+} + \cdot OH + H^+ \quad (7)$$

Roongkarn et al., (2016) reported removal efficiencies of 43.7 %, 65.9 %, and 75.8 % for heterogeneous Fenton at initial PQ concentrations of 60, 80, and 100 ppm, respectively, within 30 min at pH 3, with iron nanoparticles. In the same process, the presence of UV light provided by a 10-Watt lamp at 254 nm wavelength improves removal to 99.7 %, 84.9 %, and 69.9 % at initial concentrations greater than 100, 180, and 300 ppm, respectively, where the photo-Fenton process shows greater efficiency [24–25].

Fenton reactions are highly efficient at pH ~ 3 [16,19]. These reactions involve the addition of ferrous ions and salts, or consumption of electrical energy for the electrogeneration of Fe^{2+} [26–27]. Some methods use the acid corrosion process of metallic iron sheet surfaces in the oxidation of organic compounds [28]. Corrosion of the metal significantly increases at pH 1.5–3, which enables the *in-situ* release of iron and the occurrence of Fenton oxidation. Under acidic conditions, the metallic iron surface corrodes spontaneously as described in Eq. 8 [29], which can be more severe at high peroxide concentrations [30].

$$Fe^0 + 2H^+ \rightarrow Fe^{2+} + H_2 \quad (8)$$

Under acidic conditions, electrical energy is not required for the release of the Fe^{2+} as in an electro-Fenton processes, and the oxidation potential of the hydroxyl radical is highly favored in the oxidation reaction [31]. Galvano-Fenton is another process that uses the electrical potential differential between two metal plates (Cu-Fe) for the *in-situ* release of Fe^{2+}, reducing the addition of salts and the use of external electrical energy [32–33].

Photo corrosion of metals is possible by UV radiation at long exposure times; this phenomenon may contribute to the release of Fe^{2+} [34]. This is possibly due to two reactions mainly with photon-generated holes (h^+), and one that involves the decomposition of water to molecular oxygen (O_2) and protons (Eq. 9) [35–39] here, an aqueous medium could accelerate corrosion. In the presence of oxygen, light increases pitting corrosion by promoting the cathodic reaction on the metal surface caused by a positive photovoltage (Eq. 10). The other process directly involves the oxidation of Fe° to Fe^{2+} (Eq. 11) [34].

$$4H_2O + 8h^+ \rightarrow 2O_2 + 8H^+ \quad (9)$$

$$Fe^0 + 3H_2O + O_2 + 3h^+ \rightarrow 5OH^- + Fe^{2+} + H^+ \quad (10)$$

$$Fe^0 + 2h^+ \rightarrow Fe^{2+} \quad (11)$$

The geometry and hydrodynamic design of reactors is a major factor in their performance. A computational fluid dynamics (CFD) simulation has been used to characterize the flow pattern, to understand the hydrodynamic distribution and residence time, and to obtain the velocity and turbulence profiles [28,36–38]. The turbulence affects the speed of a reaction and studying them has enabled establishment of criteria to improve the design of reactors. It has been shown that some mechanisms promoting turbulence improve the oxidation rate in electrochemical processes [40–42]. CFD has been widely used for the modeling and improvement of diff ;erent process equipment, such as reactor, heat exchangers and centrifugal pumps, among others [43].

The novelty in this study was the development of the new Solar Corrosion Fenton (SCF) reactor. This was proposed using the zero valent iron photo corrosion in a cylindrical parabolic concentrator (CPC), promoting the *in situ* the release of the catalyst without the addition of salts or the use of electrical energy for the oxidation of PQ. The amount of metallic Fe exposed to photo corrosion, peroxide doses, hydraulic retention time (HRT), and solar UV irradiation times were evaluated for PQ oxidation through a surface response methodology. CFD study was carried out to verify the influence of the components on the flow field and turbulence.

2. Materials and methods

2.1. Reagents

Commercial PQ solutions (Gramoxone ®) were used at 100 mg L^{-1} in deionized water, as this is the maximum recommended dose [5] and it was evaluated in different studies [14]. The pH of the solutions was adjusted to 2.8 with 2 M H_2SO_4.

2.2. Analytical methods

The concentration of PQ was analyzed by high-performance liquid chromatography (HPLC) using a UV–vis detector and a Zorbax SB C18 column (250 × 4.6 mm, 5 µm, Agilent Technologies) as the stationary phase, maintained at 30 °C with a mobile phase of 95 % 10 mM ammonium acetate, 1% phosphoric acid, and 5% acetonitrile, in isocratic solution with water-grade HPLC at a flow rate of 1 mL min^{-1}. The detection wavelength was at 260 nm. The peak was found at a retention time of 2.1 min. An Agilent Technologies 1260 Infinity HPLC was used for all the experiments.

The commercial PQ solution and the treated samples were characterized to enable the comparison of results. The pH, electrical conductivity (EC), and total dissolved solids (TDS) were measured with a HANNA HI 2550 potentiometer [44]. The total organic carbon (TOC), total inorganic carbon (TIC), and total carbon (TC) were determined by

the non-purgeable organic carbon method on a Shimadzu VCPH with a detection limit = 0.05 mg L^{-1} [15]. The biochemical oxygen demand (BOD_5) and iron concentration were determined according to standard methods [45]. The chemical oxygen demand (COD) was determined by an alternative peroxide-based method [46]. The final pH was adjusted to 8.5 (with 1 M KOH), and the samples were centrifuged to avoid Fe interferences. Absorbances at 254 nm were used as an aromaticity indicator. Samples were normalized to a dilution of 1:10 using a 1 cm quartz cell and a HACH DR 6000 spectrophotometer [47]. Fe^{2+} concentrations were analyzed using the 110-phenanthroline ferrous colorimetric method at 510 nm, and Fe^{3+} was calculated as the difference from total Fe. The dose and residual peroxide (H_2O_2) concentration were adjusted using the iodometric method [48]. The HACH TNT-831 method was used for ammoniacal nitrogen (N-NH_3).

Lactuca sativa seeds were used to evaluate the toxicity and determine the effective average concentration (EC_{50}) required to inhibit the germination and hypocotyl growth ($\leq$ 2 cm) of 50 % of the exposed seeds, after 120 h compared to the controls [49]. PROBIT tests [50] were applied in the statistical program Statgraphics Centurion XVI.II.

2.3. Solar corrosion fenton process (SCF)

Fig. 1 shows the experimental unit used. The 20 cm long, 2 cm Φ Kimax borosilicate reactor showed an 88 % transmittance at 340 nm. The volume of the borosilicate reactor (V_t) (64 + 0.2 cm^3) was packed with a coiled iron filament of annealed Fe wire to different surface area (A_f) to volume (V_t/A_f) ratios. A cylindrical parabolic concentrator (CPC) with a 70° inclination was designed to concentrate solar UV light and improve the sludge precipitation due to wear and pitting of the iron filament. The CPC was built with Miro-Sun® sheet with a 93 % reflectance. The SCF reactor was operated in the continuous mode, at different HRT, and H_2O_2 was continuously dosed.

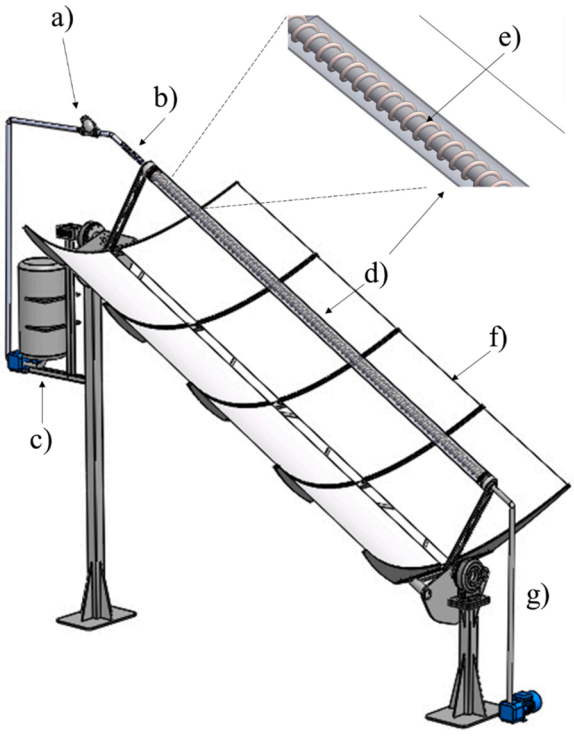

Fig. 1. Experimental solar Fenton reactor: a) influent, b) static mixer, c) peroxide feed, d) borosilicate reactor, e) Fe filament, f) reflective sheet, g) effluent.

2.4. Fe released by acid corrosion

In order to measure the corrosion rate of the filament, the SCF reactor was fed with deionized water at pH 2.8 (adjusted with 0.4 M H_2SO_4) to avoid the formation of iron oxides and promote Fenton reactions [31], and packed with V_t/A_f ratios (cm^3:cm^{-2}) of 3:1, 6:1 and 9:1. The Fe^{2+} thus released was quantified from 0−40 min of HRT, in the batch mode.

2.5. Statistical optimization process of the SCF system

A Box-Behnken design was used to determine the optimal conditions in the removal of PQ, COD, and TOC. The independent variables (factors) used in this study were the H_2O_2 concentration at 500, 1500 and 2500 mg L^{-1} (H_2O_2/PQ molar ratios: 38, 113 and 189 respectively); HRT at 20, 30 and 40 min (Reynolds numbers of 2.9, 1.9 y 1.4 respectively); and V_t/A_f ratios of 3:1, 6:1 and 9:1. The initial pH was adjusted to 2.8 and was not controlled during the process; the final pH was also measured. The software Statgraphics Centurion XVI.II was used for design, mathematical modeling and optimization of the operational parameters of the SCF system. The response surface methodology (RSM) was used to verify the influence of the different factors and their interactions during the process response [51] and to optimize operating conditions to a 99 % removal of PQ. The levels of independent variables are displayed in Table 1. Fifteen experiments were conducted in two blocks and three center point, in aleatory order.

2.6. Effect of UVA radiation on the reaction rate

The SCF reactor was operated in the continuous mode in optimized conditions, with and without solar radiation; when the reactor was operated in the dark mode, it was referred to as the Corrosion Fenton (CF) system. Samples were taken at 5−30 min of operation, and the final concentrations of PQ, CT, and COD were determined. The results were fitted to the Behnajady-Modirshahla-Ghanbery (BMG) model [7,22] and the second order model which was then used to calculate the kinetic constants (Eqs. 12 and 13):

Second-order kinetic model:

$$C_t = \frac{C_0}{(C_0 kt + 1)} \tag{12}$$

BMG model:

$$C_t = \left(\frac{t}{(m + bt)} + 1\right) C_0 \tag{13}$$

where C_0 is the initial concentration and C_t is the final concentration of PQ, COD and TOC at reaction time t; k is the reaction rate constant of the second order kinetic model; and m and b are the reaction rate constants from the BMG kinetic model. The software Statistica 10 StatSoft® was used to adjust the experimental data to the models and calculate the kinetic constants.

UVA radiation was monitored using a Vantage Pro2 weather station

Table 1
The experimental values and level of independent variables.

Factor	Units	Symbol	Level	Experimental values	Response
Hydraulic retention time (HRT)	min	A	−1, 0, 1	20, 30, 40	PQ removal (%)
Ratio (V_t/A_f ratios)	cm^3 cm^{-2}	B	−1, 0, 1	3:1, 6:1, 9:1	COD removal (%)
H_2O_2 doses	mg L^{-1}	C	−1, 0, 1	500, 1500, 2500	TOC removal (%)

equipped with a Vantage Pro 6490 UV spectrum sensor having a spectral response of 280–360 nm, a resolution of 0.1–0.19 MEDS (*minimal erythemic doses*), and a 5% accuracy [44]. The energy accumulated by the CPC was estimated using Eq. 14 [13]:

$$Q_{UVA,n} = Q_{UVA,n-1} + \Delta t_n \underline{UV}_{AG.n} \frac{A_r}{V_t} \quad (14)$$

Here, $Q_{UVA,n}$ is the accumulated energy (in $J\,L^{-1}$), $Q_{UVA,n-1}$ is the previously accumulated energy (in $J\,L^{-1}$), Δt is the sampling time (s), $\underline{UV}_{AG.n}$ is the average solar UVA radiation measured during the $\Delta t = t_n - t_{n-1}$ period in Wm^{-2}, A_r is the illuminated collector surface area of the parabolic concentrator (in m^2), and V_t is the total reactor volume (in L).

2.6.1. Infrared spectroscopy

The raw and treated samples were used to record IR spectra with an Affinity-1 S Shimadzu IR spectrophotometer in the wavenumber range of 500−4500 cm^{-1} using a transmission cell for liquids. The spectra were smoothed with a factor of 4 on a scale of 1–16 [52].

2.7. Effect of the H_2O_2:PQ ratio

Different H_2O_2:PQ relationships were evaluated for the removal and toxicity of PQ (C_t/C_0) (ratios of 0.4, 2.5, 5.9, 10, 17 and 22.5). The SCF reactor was operated in the continuous mode under optimized conditions with solar radiation.

2.8. Effect of the reactor components

To determine the contribution of each component of the SCF system to the removal of 100 % of PQ, a ratio of H_2O_2:PQ of 22.5 and an HTR of 28 min in continuous operation were applied to: a) solar radiation only (photolysis), b) solar radiation with peroxide dosing (H_2O_2/solar UV), and c) without solar radiation with packed iron filaments (CF). All conditions were compared to the SCF reactor. Samples obtained from the CF and SCF processes were characterized.

2.9. Computational fluid dynamics (CFD) of the reactor

Hydrodynamic analyses were carried out using Ansys Fluent© 19.1 software. The simulation of the reactor considered the experimental optimal operating condition of the flow rate and used the same geometry as the laboratory model. The general process for CFD analysis consists of four general stages: creation or establishment of the control domain (fluid) using CAD tools, spatial discretization of the domain (meshing), the establishment of equations, boundary conditions, and solution schemes, and finally postprocessing for visualization and analysis of the results. The reactor geometry was drawn using the AutoCAD© and SolidWorks© programs, and it was subsequently imported into the ANSYS program for analysis. To analyze the prototype of the SCF reactor, the recommendations issued by the National Aeronautics and Space Administration (NASA) in the NPARC Alliance Verification and Validation file were used to guarantee the accuracy of the numerical analysis.

The CFD analysis was used to verify the influence of the components on the flow field and turbulence as well as to verify the design and thus the transfer of mass in order to improve the time and removal efficiency. The optimal geometry of the mixer was established to guarantee the effect of turbulence over the entire length of the reactor in accordance with the optimal design characteristics. The simulation was performed considering the optimal SCF operating conditions, standard atmospheric pressure, inlet temperature of 20 °C and outlet temperature of 82 °C, and water density of 998.2 kg m^{-3}. The mesh was made with 0.25 mm tetrahedral elements in size with of 1 mm. The minimum orthogonal quality of the mesh was 0.16. The average quality of the elements was 0.8. These values verify good overall mesh quality according to the recommended 0.1–1.0 scale where 1 represents the maximum mesh quality [37]. The most important conditions, models, solution diagrams and parameters established for CFD simulation are presented in the Supplementary materials A.

3. Results and discussion

3.1. Characterization of the paraquat solution

A commercial herbicide (Gramoxone®) solution with 104.6 mg L^{-1} of paraquat was used for all tests, with a COD of 1277 mg L^{-1} and BOD_5 of 6.4 mg L^{-1}, a biodegradability index (BI) of 0.0050 (Table 2), TOC of 93.5 mg L^{-1} and NH_3-N of 0.26 mg L^{-1}. The difference between the concentration of PQ (active ingredient), TOC and COD, is due to the presence of other additives in the commercial herbicide [22].

The COD measured (1277 mg L^{-1}) shows that the concentration of PQ (104 mg L^{-1}) has an organic load approximately 10 times than expected, where other compounds present in the commercial herbicide such as surfactants, colorants, diluents, humectants and stabilizers contribute to a higher organic load. As the manufacturer indicates, 25 % of its composition is the active ingredient and 75 % are inert ingredients [6].

Biological treatments are not very effective in the removal of organic compounds with a very low BI [33]. Biological methods are normally susceptible to toxic compounds, which decrease microbiological activity [53]. The average inhibitory toxicity of the solution (Ec_{50}) was 25.1 mg L^{-1} PQ (Table 2), and therefore this concentration is sufficient to prevent germination and growth of half the population of exposed seeds. However, the concentration of inhibitors depends on the species exposed. Kanno et al., (2019) showed that there is a difference between the susceptibility of different cell lines to PQ and their resistance and inhibition [54]. Other studies indicate that 0.5–1.0 mg L^{-1} of PQ were specific to inhibit the activity of liver enzymes in fish, and the effect depends on the exposure time [55], which may suggest bioaccumulation processes.

3.2. Fe^{2+} released: effect of corrosion

The concentration of Fe^{2+} released by the SCF reactor is shown in Fig. 2; it shows that the concentration is directly proportional to the exposure time. The maximum concentrations released were 78.8, 69.7 and 23.7 mg L^{-1} of Fe^{2+} when the V_t/A_f ratios were 3:1, 6:1 and 9:1

Table 2
Physicochemical characterization, toxicity and operational conditions.

Parameter	Units	PQ solution	SCF	CF
pH		2.8 + 0.0	4.1 + 0.2	3.2 + 0.0
EC	μS cm^{-1}	186.3 + 1.6	246.4 + 0.3	124.2 + 1.4
Paraquat	mg L^{-1}	104.6 + 2.3	0.1 + 0.0	30.1 + 0.7
BOD_5	mg L^{-1}	6.4 + 0.5	12 + 0.7	8.4 + 1.1
BOD_5/ COD		0.0050 + 0.0	0.2058 + 0.0	0.0461 + 0.0
COD	mg L^{-1}	1277.0 + 107.5	58.3 + 0.3	182.4 + 1.6
NH_3-N	mg L^{-1}	0.26 + 0.02	5.0 + 0.1	0.48 + 0.02
TC	mg L^{-1}	93.6 + 4.4	69.1 + 0.5	69.80 + 0.3
TIC	mg L^{-1}	0.3 + 0.1	21.7 + 0.1	5.9 + 0.1
TOC	mg L^{-1}	93.5 + 4.6	47.4 + 0.5	63.9 + 0.2
Toxicity	Ec_{50} mg L^{-1}	25.1 + 1.5	0.0 + 0.0	0.0 + 0.0
SUVA at 254 nm		1.0340 + 0.0	0.0773 + 0.02	0.1942 + 0.02
Fe	mg L^{-1}	0.0 + 0.1	66.0 + 0.3	7.7 + 0.2
Fe^{2+}	mg L^{-1}	0.0 + 0.0	62.1 + 0.4	4.1 + 0.1
Fe^{3+}	mg L^{-1}	0.0 + 0.1	4.0 + 0.1	3.6 + 0.1
Residual H_2O_2	mg L^{-1}	–	7.2 + 3.4	289.2 + 27.3
Ratio H_2O_2: Fe^{2+}	–	–	36.2	547.1
Ratio H_2O_2: PQ	–	–	22.5	22.5
Ratio PQ: Fe^{2+}	–	–	1.6	24.3
Q_{UVA}	kJ L^{-1}	–	1554.7	0.0

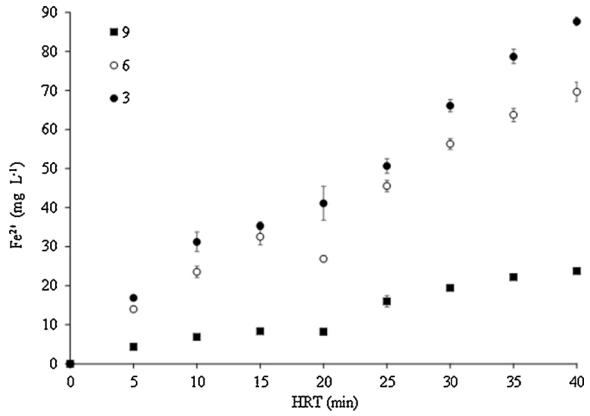

Fig. 2. Fe^{2+} released by acid corrosion at three different V_t/A_f ratios (cm^3 cm^{-2}): 3:1(●), 6:1(○) and 9:1(■).

respectively, with a hydraulic retention time of 40 min. In addition, the results showed that the amount of Fe^{2+} released is dependent on the amount of packed iron filament, because there is a greater surface area of the filament exposed to corrosion (21, 11 and 7 cm^2 respectively). Namkung et al., (2010) demonstrated that total Fe release by acid corrosion increases steadily over time.

At 20 min of HRT a significant difference in the release of Fe^{2+} is observed between the relations 3:1 and 6:1 (Fig. 2). For this reason, during the optimization process, the selected times were 20, 30, and 40 min. Santo et al., (2011) evaluated the removal of PQ using a classic Fenton (CF) process using 27.9 mg L^{-1} of Fe^{2+}. In an electro-Fenton process, 11.2 mg L^{-1} of Fe^{2+} [19] and 11.8 mg L^{-1} of Fe^{2+} were used in the photo-Fenton process [13]. Therefore, the release of ferrous ions obtained by the SCF reactor is above the minimum used by other authors in the removal of PQ.

3.3. Optimization of the SCF process

3.3.1. PQ removal

Table 3 shows the experimental matrix design for SCF optimization, where the main variables studied were HRT, V_t/A_f ratios (cm^3 cm^{-2}) and H_2O_2 concentration. The response variables were %PQ, %COD and % TOC removals; in addition, the consumption was also monitored.

To study the interaction of the different variables in the optimization of the SCF process, response surface plots were constructed. Fig. 3 shows the response surface for the removal of PQ from a commercial formulation. In a), the interaction between V_t/A_f ratio (cm^3 cm^{-2}) and H_2O_2 concentration is presented. At a higher concentration of H_2O_2, the removal increases because a greater amount of hydroxyl radicals is generated (Eq.1). When the V_t/A_f ratio decreases and a larger amount of Fe filament is packed, a maximum efficiency is obtained with a lower concentration of H_2O_2. This is possible according to Eqs. 1 and 7, where radical formation is catalyzed by ferrous ions [21].

Fig. 3b shows the HRT and H_2O_2 interaction where the maximum efficiency is obtained by increasing the peroxide dosage. According to the analysis of variance (ANOVA) in Table 1B (Supplementary material), the HRT factor does not have a significant effect on the removal of PQ, because P is greater than 0.05. The HRT and the V_t/A_f ratio interaction is presented in Fig. 3c, and shows that when the ratio volume:surface decreased, the PQ removal increased. However, the ANOVA (Table 1B Supplementary material) indicates that the interaction does not have a significant effect on herbicide removal with a probability $p > 0.05$. The equation and the adjustment of the response surface model are presented in Supplementary material B.

The optimal conditions for the removal of PQ in the SCF reactor were: 2248.7 mg L^{-1} of hydrogen peroxide with a molar ratio of 170 H_2O_2:PQ, an HTR of 28 min and a volume: surface area ratio of 3.4:1. These conditions resulted in 100 % removal of PQ, as determined by HPLC (Table 4 and Fig, 3). The optimal conditions of the SCF process to obtain the 100 % of removal of PQ result in an excessive reagent consumption; however, the high concentration of generated radicals allows

Table 3
Experimental matrix design for optimization of SCF.

Run #	Block	Factor			Response			
		HRT (min)	Ratio (cm^3 cm^{-2})	H_2O_2 (mg L^{-1})	% PQ removal	% COD removal	% TOC removal	Consumption of H_2O_2 (%)
1	1	20	3:1	1500	99.9	87.0	63.3	98.7
2	1	40	3:1	1500	99.9	85.8	68.2	99.4
3	1	20	9:1	1500	91.1	81.0	77.9	100.0
4	1	40	9:1	1500	88.8	91.5	77.6	100.0
5	1	20	6:1	500	58.0	34.0	39.3	90.0
6	1	40	6:1	500	39.5	38.4	41.0	100.0
7	1	20	6:1	2500	99.9	75.5	78.0	92.3
8	1	40	6:1	2500	99.9	99.6	79.1	96.9
9	1	30	3:1	500	99.9	80.6	71.3	100.0
10	1	30	9:1	500	37.0	35.6	47.1	100.0
11	1	30	3:1	2500	99.9	92.9	90.2	76.8
12	1	30	9:1	2500	90.4	93.7	97.5	91.5
13	1	30	6:1	1500	86.6	75.1	68.5	99.9
14	1	30	6:1	1500	81.5	78.0	73.2	99.9
15	1	30	6:1	1500	95.0	76.5	72.9	99.9
16	2	20	3:1	1500	99.9	91.0	64.8	99.4
17	2	40	3:1	1500	99.9	85.3	65.8	99.4
18	2	20	9:1	1500	92.2	78.3	71.6	100.0
19	2	40	9:1	1500	86.2	90.7	75.7	100.0
20	2	20	6:1	500	57.5	36.6	43.7	100.0
21	2	40	6:1	500	58.6	39.7	44.0	100.0
22	2	20	6:1	2500	99.9	77.2	80.0	88.4
23	2	40	6:1	2500	99.9	100	82.6	96.1
24	2	30	3:1	500	99.9	81.4	71.0	100.0
25	2	30	9:1	500	40.4	34.6	43.9	100.0
26	2	30	3:1	2500	99.9	92.8	88.9	84.6
27	2	30	9:1	2500	91.0	93.6	95.9	88.7
28	2	30	6:1	1500	88.2	72.9	71.1	99.9
29	2	30	6:1	1500	75.7	72.9	73.0	99.9
30	2	30	6:1	1500	88.2	91.0	73.0	99.9

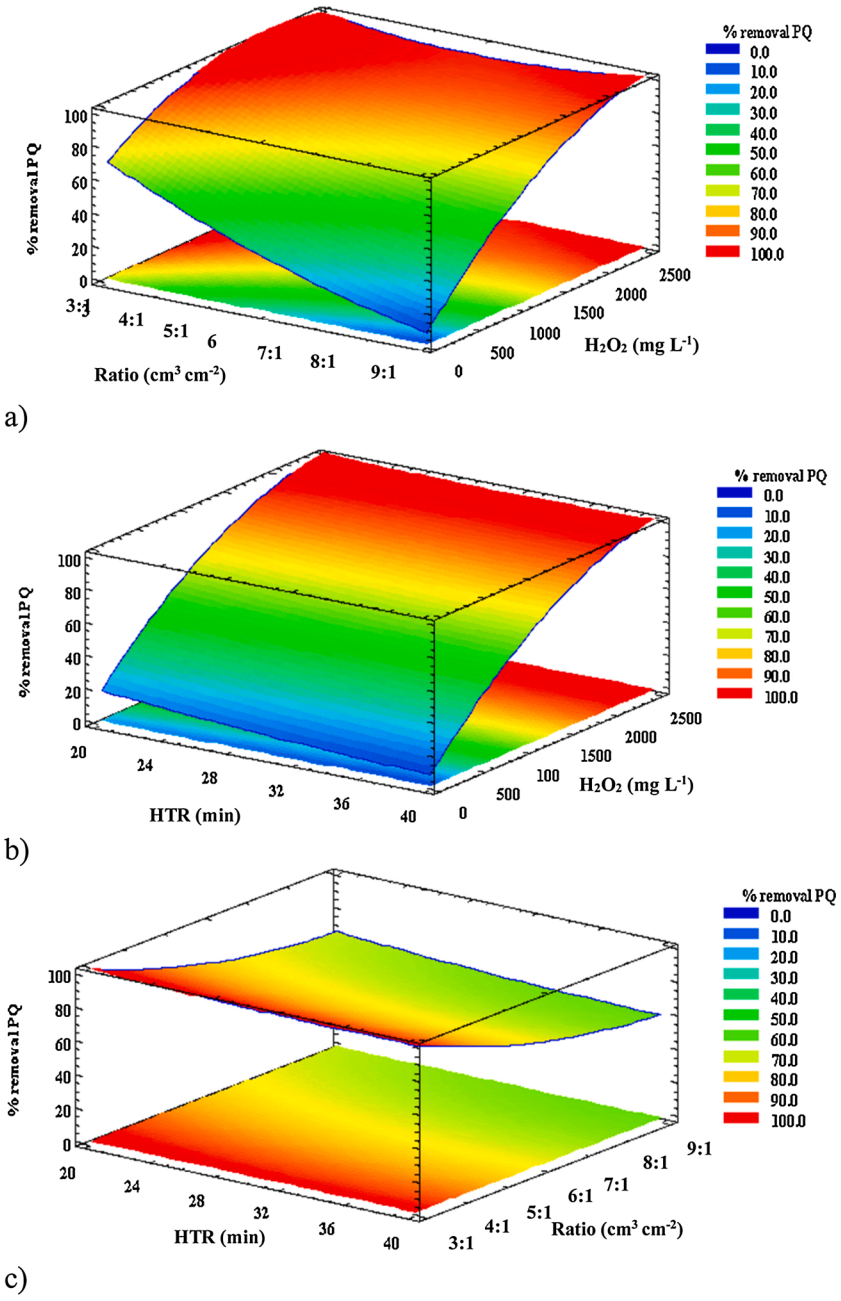

Fig. 3. Surface response plots for PQ removal determined by HPLC, a) interaction between the V_t/A_f ratio and H_2O_2, b) interaction between HRT and H_2O_2 and c) interaction between HRT and Ratio.

Table 4
Optimum conditions found, using design expert program.

Response	H_2O_2 (mg L^{-1})	HRT (min)	Ratio (cm^3 cm^{-2})	% removal(Observed)	% removal (Predicted)	Molar ratio(H_2O_2:PQ)	R^2	**STD**
% removal PQ	2248.7	28.0	3.4:1	99.9	93.8	170.0	0.8749	8.7
% removal COD	2456.6	29.3	8.8:1	100	93.9	185.7	0.9224	7.2
% removal TOC	2451.6	29.2	8.8:1	96.7	100.0	185.3	0.9369	2.0

for significant reduction of treatment time (28 min), which results in the reduction of the consumption of electrical energy.

Trovó et al., (2013) obtained a removal of 64.6 % of commercial PQ by applying a photo-Fenton process with an initial concentration of PQ 50 mgL^{-1}, 11.8 mg L^{-1} of Fe^{2+}, and 188.1 mg L^{-1} of H_2O_2 in 60 min of treatment time.

Dhaouadi et al., (2009), achieved a 94 % PQ removal during its treatment at an initial concentration of 20 mg L^{-1} with the electro-Fenton process; 200 mA were applied for 60 min, with 0.2 mM of Fe^{2+}. Badli et al., (2017), studied the photocatalysis using a ZrO_2:TiO_2 ratio of 20:80, with 0.3 g of catalyst in 250 mL. This approach yielded 84.4 % of PQ degradation with the application of UV radiation for 240 min, at 15 ppm of the PQ herbicide [56]. On the other hand, Zahedi et al., (2015) used applied photocatalysis with Ti_2O nanoparticles to

obtain 84.4 % PQ removal in 5 h of visible light radiation with an initial concentration of 10 ppm and pH 5.8. Cartaxo et al., (2015) applied an electro oxidation process, obtaining 79 % of PQ removal in 1.5 h and 64 % in 3 h of electrolysis, using Pt/steel and Co_2FeO_4/Co_2FeO_4 electrodes respectively at 0.1 A, in 100 mL of solution.

3.3.2. COD removal

The performance of the SCF reactor in COD removal is shown in Fig. 4 a–c, where the interactions of the evaluated factors are observed. The factor that had the greatest effect on COD removal was the concentration of dosed H_2O_2 (Table 2A), according to ANOVA. The highest removal efficiency (Table 4: 100 % + 7.2) was obtained with a higher ratio volume: packed filament surface (Fig. 4a). As shown in Fig. 2, this high ratio corresponds to the lowest Fe^{2+} concentration.

The initial value of the COD of the commercial herbicide used in this research was 1277 mg L^{-1} (Table 3). In the optimization tests, 100 % was removed in 29.3 min with a V_t/A_f ratio of 8.8:1 and a dose of 2456.6 mg L^{-1} of H_2O_2, with a molar ratio of 185.7 H_2O_2:PQ (Table 4 and Fig. 4). The initial concentration of COD was higher than in other investigations, and the treatment time was significantly shorter. However, the concentration of H_2O_2 used was considerably higher. In the commercial herbicide, there are other organic compounds such as surfactants and dyes, that also consume hydroxyl radicals; consequently, a greater amount of H_2O_2 must be dosed.

The HRT:H_2O_2 interaction shows that the percentage of peroxide consumption increases with increasing treatment time, as show in Table 3. The percentage of H_2O_2 consumption increases with increasing time; in the tests, a low concentration of residual H_2O_2 was observed.

In the HRT and V_t/A_f ratio interaction, there was no significant effect on COD removal (Fig. 4c) according to the ANOVA in Table 2A. It is possible that this lack of effect is due to the high concentration of Fe^{2+} and the reaction time. The equation and the adjustment of the response surface model are presented in Supplementary material B.

Dhaouadi and Adhoum (2009) evaluated an electro-Fenton process

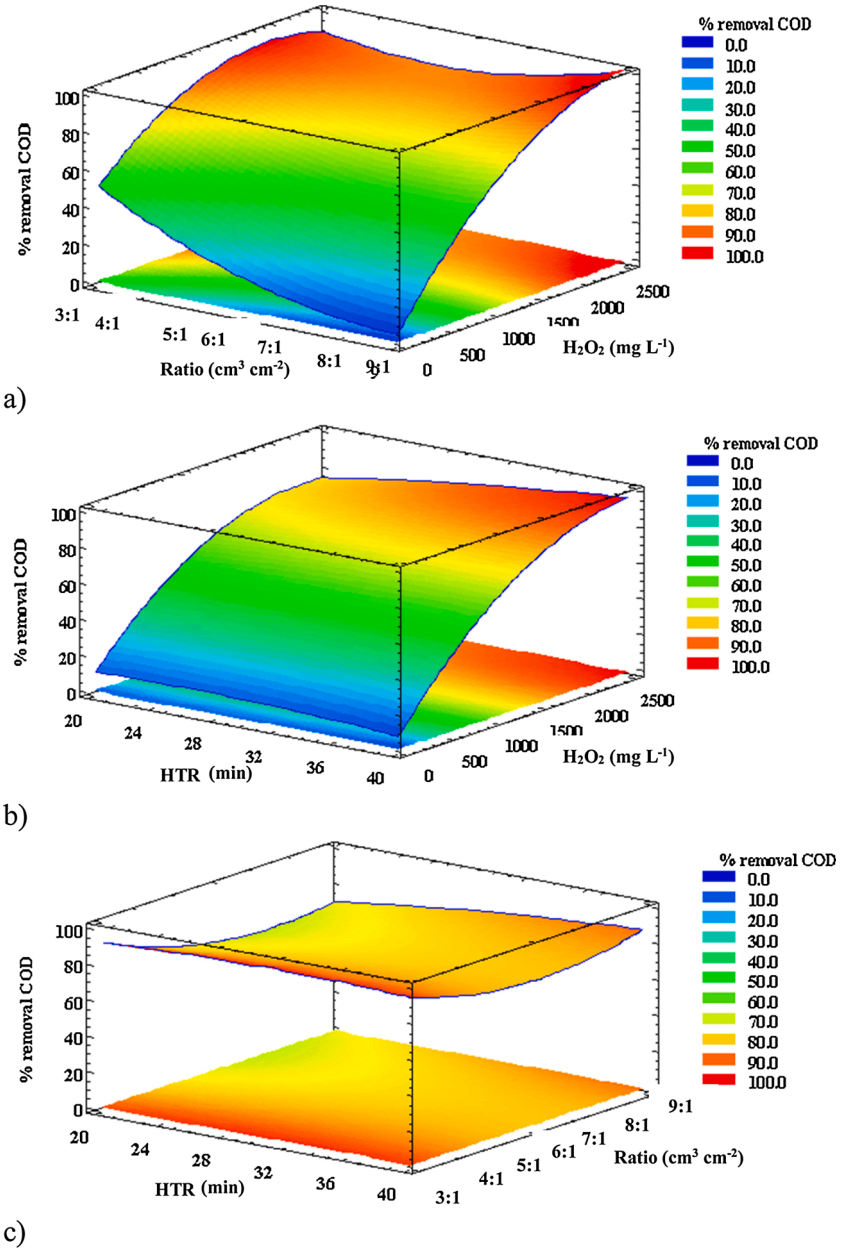

Fig. 4. Surface response plots for COD removal: a) interaction between V_t/A_f ratio and H_2O_2, b) interaction between HRT and H_2O_2 and c) interaction between HRT and V_t/A_f ratio.

with a removal efficiency of 94 % of COD ($COD_0 = 38.6\ mg\ L^{-1}$) of an analytical grade PQ ($PQ_0 = 20\ mg\ L^{-1}$) solution, using an Fe^{2+} concentration of 11.2 mg L^{-1}, and current intensity of 100 mA for 480 min. The SCF process is attractive for improving the removal of the contaminant at higher concentrations, without using electrical energy and in a significantly shorter time.

3.3.3. TOC removal

Fig. 5a shows the interaction between V_t/A_f ratio and H_2O_2, where the maximum TOC removal efficiency was achieved using a higher concentration of H_2O_2. The highest removal efficiency was 96.7 % + 2 (Table 4) using a peroxide concentration of 2451.6 mg L^{-1}, with a molar ratio of 185.3 H_2O_2:PQ, 29.2 min, and a V_t/A_f ratio of 8.8:1 (Table 4). Marien et al., (2018), evaluated the removal of PQ by photolysis and photocatalysis, using SiC foams with P25-TiO_2 nanoparticles deposited by immersion and obtained 4 and 91 % of TOC removed after 3 h of treatment, respectively [15]. The optimal time in the SCF process is significantly shorter; however, to obtain a greater efficiency the amount of peroxide used must be higher.

Table 3B (Supplementary material) indicates that the HRT:H_2O_2 interaction (Fig. 5b) does not have a significant effect on the response variable (TOC), because $p > 0.05$. HRT has a directly proportional effect on the Fe^{2+} content; however, it does not have a significant effect on the removal of TOC. The interactions represented in Figs. 5b-c do not present a significant effect on TOC removal, and therefore a uniform behavior is observed. In addition, the ANOVA shows that peroxide concentration is a strongly influential factor ($p = 0.00$) in the removal of TOC; it increases with increasing peroxide dose.

The interaction HRT:V_t/A_f ratio (Fig. 5c) does not have a significant effect on the response variable (TOC) (Table 3B: $p = 0.2731$). However, these two factors have a directly proportional effect on Fe^{2+} content (Fig. 2), and the TOC removal efficiency decreases when the release of iron increases. Other authors have used concentrations of 11.2, 11.8 and 27.9 mg L^{-1} of Fe^{2+} to remove of PQ through Fenton reactions [7,9,31].

3.4. Kinetics

The kinetic parameters in the degradation of PQ under optimal conditions were fitted as a function of the second order reaction and BMG models [9]. This model has been applied in Fenton reactions [6,7,

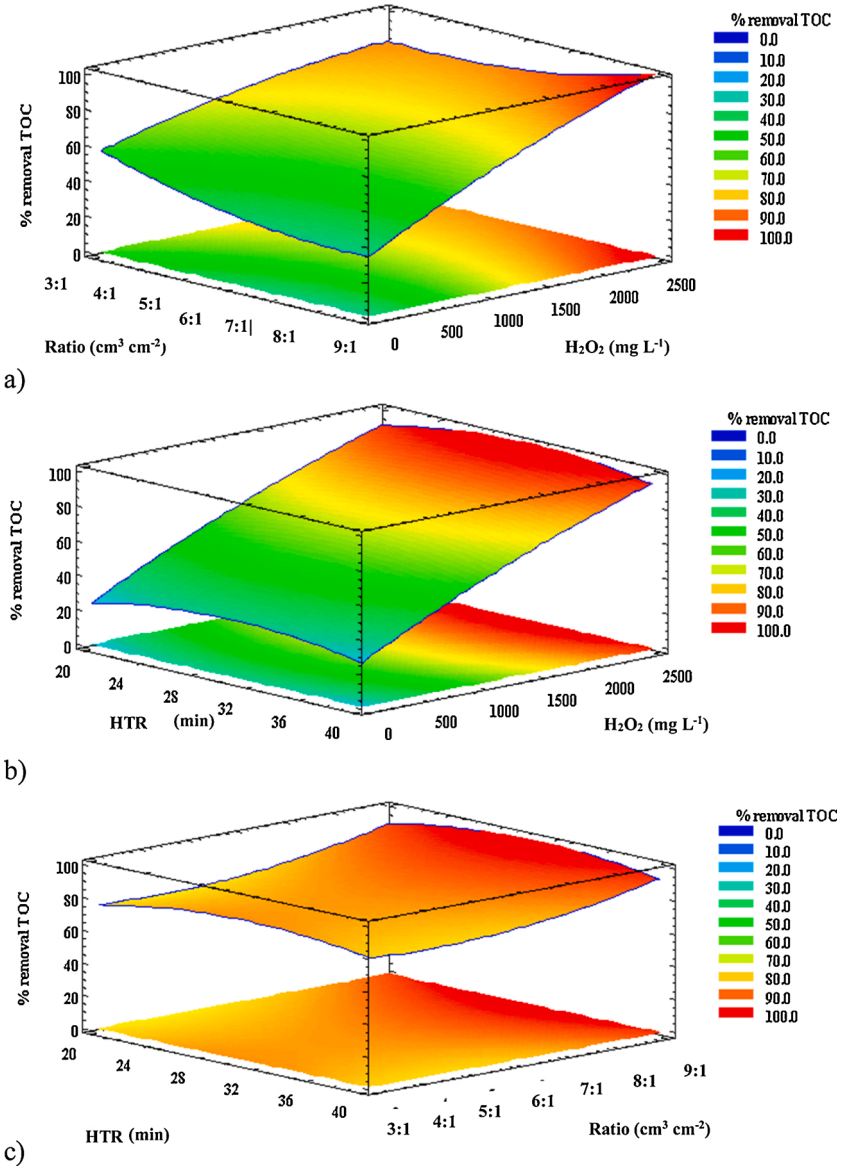

Fig. 5. Surface response plots for TOC removal: a) interaction between the V_t/A_f ratio and H_2O_2, b) interaction between HRT and H_2O_2 and c) interaction between HRT and the V_t/A_f ratio.

18,32]. Table 5 shows the kinetic constants and the correlation coefficients (R^2). The second order model does not present a good fit compared to the BGM model; the latter was the best model for describing removal in the SCF process. The kinetic constants *m* and *b* (Table 5) indicate the initial removal rate and the theoretical maximum removal [9] of PQ, TOC and COD. A low value of *m* indicates a rapid removal, so the SCF process was more efficient in removing PQ and TOC. In its first stage, the BMG model describes the maximum rate of PQ removal, which may be related to the reduction of the pyrimidine group, followed by the degradation of the carboxylic acids formed [57–59]. The SCF process allowed a 100 % degradation at an initial concentration of 100 mg L^{-1} PQ (Table 4) in 28 min of treatment with doses of 2248.7 mg L^{-1} H_2O_2 with 62.1 mg L^{-1} iron released at a ratio of 3.4:1 cm^3 cm^{-2}. The final mathematical expression obtained for the initial removal rate and the maximum theoretical removal as a function of the *m* and *b* constants are presented in the Supplementary materials, Table C1.

Badli et al., (2017) determined the kinetic constants in the degradation of PQ through a photocatalytic process using ZrO_2/TiO_2. The fitted model was pseudo first order, k =0.0056 min^{-1}, with a C_0 = 15 ppm and a total time of 180 min. Although the kinetic models are different, the treatment time was significantly shorter in the SCF process. The efficiency of the process may be related to the design, volume, and type of solar concentrator used.

The constant *m* in the removal of PQ and TOC was significantly lower in the SCF process (0.4713 and 1.7891 respectively) than in the CF (2.3683 and 2.6971 respectively) (Table 5), because of the solar radiation improves the reaction rate, increasing the generation of hydroxyl radicals [60–63]. However, for COD the constant *m* was higher in the SCF process, which shows that the reaction rate was lower than in the CF process. According to the results shown in Table 2 the release of Fe was significantly higher in the SCF process where the formation of by-products [63,64] and the high concentration of Fe, could possibly favor the formation of organometallic complexes [33], which increased the COD in the SCF process, even though iron was precipitated and removed from the sample. The formation of by-products is supported by the high values of the constant *m* in the removal of TOC (1.7891) compared to the removal of PQ (0.4713) in the SCF process, which indicates that the mineralization rate is slower.

3.5. Effect of solar UV light

Fig. 6 shows the effect of UV-A radiation on the elimination of PQ, COD and TOC from the commercial herbicide evaluated at 30 min of operation. The best fitted model was BMG and the accumulated energy obtained in the SCF process was 1554.7 kJ L^{-1}. PQ removal was stable after 10 min, with and without the presence of UV-A radiation; however, solar radiation improves removal efficiency between 10–30 % at pH 2.8. In this way, Umar et al., (2010) concluded that the efficiency in COD elimination from a photoelectro-Fenton process is 10 % higher compared to an electro-Fenton. The accumulated energy obtained has a direct effect on the removal of pollutants [47], and therefore 1554.7 kJ L^{-1} (Table 2) was necessary for 100 % removal of the PQ, which will depend strongly on the weather station [33]. Other authors have obtained 64 % removal of a 50 mg L^{-1} solution of commercial PQ by a photo-Fenton process, obtaining an accumulated energy of 642 kJ L^{-1} in 60 min of treatment by dosing 188.1 mg L^{-1} of H_2O_2 at pH 2.5–2.8 and Fe^{2+} of 11.8 mg L^{-1} [13].

The highest percentage of PQ degradation occurs in the first 10 min of reaction; however, a longer time and more accumulated energy are necessary to reach the optimum value, possibly due to the presence of byproducts and other organic compounds in the commercial herbicide

Table 5
Kinetic parameters and determination coefficient for PQ, TOC and COD removal in a Gramoxone herbicide.

Parameter	Processes	Second order k_2 (L mg^{-1} min^{-1})	R^2	BMG m (min)	BMG b	BMG R^2
Paraquat	SCF	0.0047	0.9773	0.4713	1.1548	0.9985
	CF	0.0015	0.9488	2.3683	1.3390	0.9916
TOC	SCF	0.3909	0.9697	1.7891	1.0673	0.9727
	CF	0.0837	0.8805	2.6971	1.5955	0.9910
COD	SCF	0.0005	0.9976	1.6449	0.9755	0.9981
	CF	0.0005	0.9884	0.4590	1.1020	0.9981

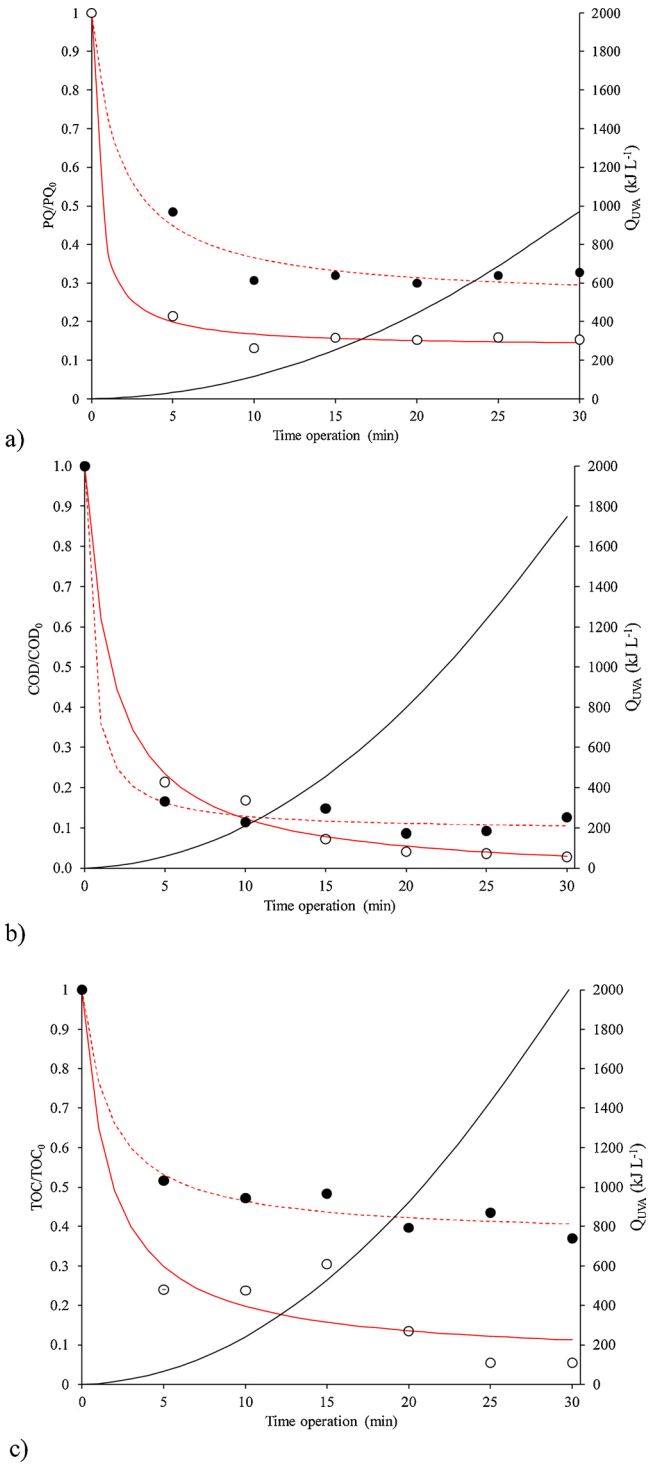

Fig. 6. Kinetics fitted by the BGM model (red line), of a) PQ, b) COD, and c) TOC removal; experimental data of solar UV light (○ with solar UV light, ● without solar UV light) and accumulated energy (black line).

[22]. The effect of UV light on COD removal (Fig. 6b) resulted in significant changes after 15 min of reaction, where the presence of UV light improves the removal by 10 %. The removal of TOC (Fig. C) improved between 20–30 % with the presence of solar UV light; the maximum removal is obtained at 25 min of reaction, when the accumulated energy was greater. The results of this research show a 94.5 % removal of TOC (Fig. 6c) with an accumulated energy of 2021 kJ L^{-1}. Trovó et al., (2013) obtained an 89 % TOC removal with an accumulated energy of 1284 kJ L^{-1}. The high energy obtained by the SCF reactor may be related to the volume of operation; the accumulated energy was calculated at different A_r/V_t ratios under the same effect of solar radiation (Supplementary material Fig. 1D). According to Eq. 14, at a lower volume the greater the accumulated energy. To achieve high energy, the A_r/V_t ratio must be ≥ 1.

The amount of Fe^{2+} released depends directly on the HRT and the amount of Fe filament packed (Fig. 2). Optimization tests indicated that a time of 28 min of HRT was necessary to remove 100 % of the PQ, obtaining an amount of 62.2 mg L^{-1} of Fe^{2+} released which was consistent with the expected results of Fig. 2 which shows that the Fe dose remained constant. Finally, a H_2O_2:Fe^{2+} ratio of 36.2 was significantly lower than that obtained in the CF process (Table 2), which could strongly influence the removal efficiency. The difference between the total Fe released may be related to the effect on UV-A radiation. According to Burleigh et al., (2003), the SCF process could favor a photo corrosion of the metal. Although this phenomenon has been reported in prolonged time exposures, it is possible that the CPC and the characteristics of the problem solution accelerated the release. The greater amount of total Fe released could be promoted by photo corrosion (Eqs. 9–11) and to a lesser extent by acid corrosion.

Fig. 6c shows a slight increase in TOC at 15 min when solar radiation (SCF) is applied. This may be related to the formation of iron hydroxocomplexes between Fe^{2+} and the by-products of PQ degradation that can increase TOC value. After this time, the complexes are broken and the mineralization continues, thus decreasing the TOC concentration [33].

3.5.1. FT/IR spectra

Fig.7 shows the infrared spectra of the PQ standard, Gramoxone herbicide and treated samples under the optimal conditions of the SCF and CF reactor. a) The main PQ standard bands were observed at 3520 and 3344 cm^{-1} that represent the stretching vibration of aromatic amines (N—H), at 2960 and 2925 cm^{-1} that represent the stretching of the C—H of aromatic rings, at 1640 cm^{-1} representing the stretching of C═N and C—N bonds, at 1513 cm^{-1} representing weak deformation of CH_3–N^+ bonds, and at 1986, 1860, 1730 and 847 cm^{-1} that represent the deformation of para-substituted aromatic rings of the herbicide [28, 34].

b) Gramoxone herbicide exhibits characteristic bands of the PQ STD centered at 3520, 3347, 2960 and 2925 cm^{-1} for sp^3 C—H stretching with a displacement in relation to the standard, at 1679 and 1513 (stretching of C═N and C—N bonds, respectively), and at 1923, 1870, 1735 and 879 cm^{-1}. The bands between 2700 and 2400 may indicate the presence of -SH or bisulfate ion bonds due to the pH of the sample adjusted with sulfuric acid [41]. The difference between the signals shown by the standard and the commercial herbicide may be due to the presence of other adjuvant organic compounds [42].

In the SCF treatment sample (Fig. 7c), the signals at 3344 cm^{-1} and 1640 cm^{-1} decrease in intensity. The absence of the signals at 1860 and 847 cm^{-1} shows the rupture of the link in the *para-* position of the aromatic ring. It is possible that, under the experimental conditions evaluated, the partial decomposition of PQ occurred. This was probably due to rupture of the main structure allowing the formation of short chain compounds such as carboxylic acids [11]. This is due to the specific UVA of the SCF treatment (Table 2) which decreases dramatically, qualitatively indicating the degradation of ring structures. Although the intensity in the signals of aliphatic groups decreased, it is possible that

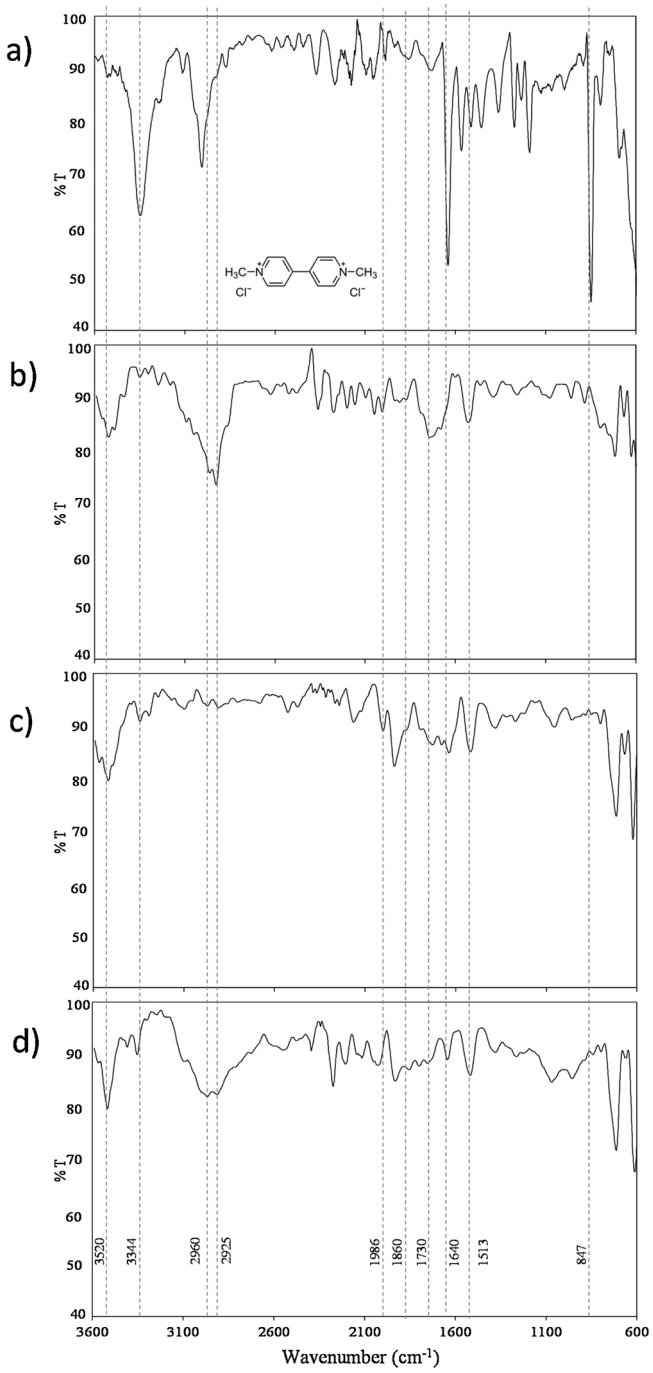

Fig. 7. Infrared spectra of a) standard PQ, b) Gramoxone (pH 2.8), c) SCF treatment (pH final 4.1) and d) CF (pH final 3.2) treatment. Experimental conditions: 2248 mg L^{-1} H_2O_2, *V/A* ratio of 3.4:1, HRT 28 min, initial pH 2.8.

the increase in BOD_5 (Table 2) may be due to the decrease in toxicity and the formation of easily biodegradable structures [33]. The 3292 cm^{-1} signal indicates a high concentration of NH_4^+ (Fig. 7 c) due to the stretching of NH_2 from primary amines. It is possible that the degradation of the herbicide allows the release of ammoniacal nitrogen form which increases its value from 0.26 to 5 mg L^{-1} (Table 2). Finally, the effect of solar UV light allows the degradation of the PQ structure with greater efficiency. In the CF treatment (Fig. 7 d) the signals of the aromatic *p*-substituent position decrease (1929, 1854, 1748, 839 cm^{-1}), but they remain as aliphatic groups (2966 and 2909 cm^{-1}) and the links C═N (1516 cm^{-1}) and C═C bonds (1640 cm^{-1}), which are also present.

3.6. Effect of the H_2O_2:PQ ratio in the toxicity removal

Under optimal conditions, the effect of the H_2O_2:PQ ratio was evaluated for the removal of PQ and toxicity. The results are presented in Fig. 8. A total of 90 % of PQ removal was obtained with a ratio of 10, using 1200 mg L^{-1} of H_2O_2. To obtain a complete removal (100 % PQ), 2248 mg L^{-1} of H_2O_2 would be necessary. The difference may be due to the presence of other adjuvant organic compounds that are mixed with the active substance and that are present in the commercial herbicide. In the degradation process they also consume radicals [7,36], and thus the degradation reactions are possibly removing other organic compounds and byproducts of the PQ oxidation.

However, 100 % of the toxicity was removed at a 5.9 H_2O_2: PQ ratio, adding 700 mg L^{-1} of H_2O_2. Therefore, a lower concentration was necessary. Based on the biological model used in the toxicity tests, a concentration greater than 25.1 mg L^{-1} (Table 2) of PQ (EC_{50}) is necessary for a 50 % inhibition in *Lactuca sativa* seeds. Thus, when the concentration is below this threshold, the toxic effect of PQ is completely removed.

According to Trovó et al., (2013), 87 to 33 % toxicity was removed from the inhibition of *Artemia saline* mobility when the concentration of PQ (C_0 = 50 mg L^{-1}) was reduced. By removing 89 % of TOC, the toxicity was reduced to 20 %. Consequently, the sensitivity in the herbicide toxicity response is different in each species. In *Vibrio sp*, a greater susceptibility has been observed upon reduced enzymatic activity of superoxidase dismutase [60,61]. Gonzalez-Cuna et al., (2016), demonstrated that microbial communities are susceptible to changes in the predominant species when they are subjected to different concentrations of herbicides. Therefore, evaluations with other living organisms must be carried out and adapted to particular conditions.

3.7. Effect of the components

Fig. 9 shows the removal of PQ through photolysis (solar UV only), H_2O_2/solar UV, CF, and SCF, where 0.5 % removal is obtained by photolysis in the absence of iron and hydrogen peroxide. Therefore, the Gramoxone herbicide showed high persistence against the photolytic effect using CPC, although some authors claim that the PQ is photochemically decomposed by ultraviolet radiation in aqueous solution [62,63]. Possibly some of the adjuvant components in the herbicide formulation may improve the solubility and stability of the active ingredient [36,38], which confers high persistence to the photolysis treatment. The H_2O_2/solar UV system in the absence of catalyst (i.e., by corrosion), only achieved 21 % PQ.

On the other hand, corrosion Fenton (CF) in the absence of UVA light at pH 2.8 achieved a 71 % PQ removal in 28 min.

Finally, SCF achieved 100 % PQ removal because solar UV radiation allows photoreduction of the catalyst by increasing the formation of radicals. The SCF reactor operated with 28 min of HRT, a dose of 2248 mg L^{-1} of H_2O_2 and a V_t/A_f ratio of 3.4:1, and this combination

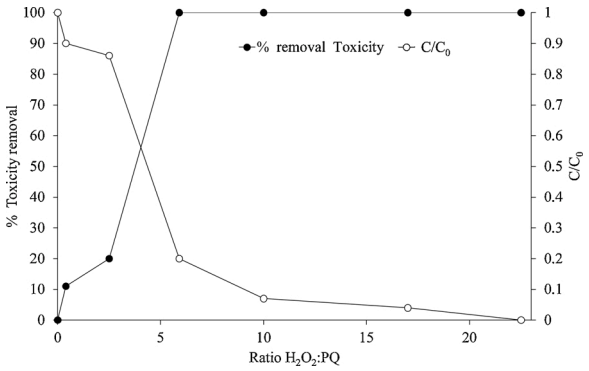

Fig. 8. Toxicity removal at different ratios H_2O_2:PQ.

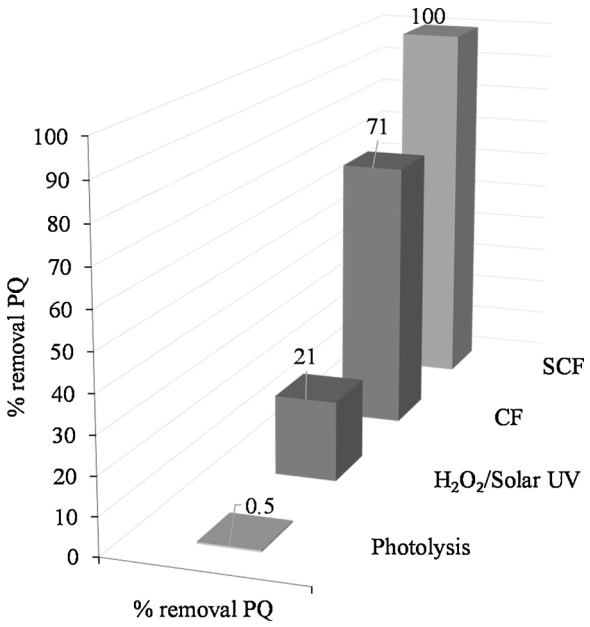

Fig. 9. PQ removal by SCF reactor components.

yielded a 100 % removal of Gramoxone PQ. Due to the greater amount of the peroxide dosed (Table 2), the reactor design enabled an increased production of hydroxyl radicals, which increases the removal efficiency and the treatment time, using natural UV light and by metallic corrosion. Iron was dosed *in-situ*, and so additional iron salts were not necessary.

3.8. CFD model

The results of the CFD hydrodynamic analysis are shown in Fig. 10 A. The outline of total velocity in the reactor is presented from the inlet to the outlet. The velocity at the inlet (which is approximately 0.5 mm s^{-1}) increases in the static mixer area to 1 mm s^{-1}. This effect allows the flow to mix before entering the reactor with turbulence, ensuring the contact of the dosed peroxide with the PQ solution. The speeds are lower inside the reactor due to the increase in the diameter of the reactor [64]. Therefore, the geometry of the SCF reactor does not cause a significant increase in flow patterns and turbulence. Removal efficiency may be largely related to the system's ability to generate hydroxyl radicals.

Increasing turbulence could increase mass transfer, and this possibly improves reaction rates [52]. However, an excessive turbulent pattern can result in areas with a higher catalyst concentration by surface detachment of the pit by corrosion [27], which could influence the generation of areas of high iron release. An excessive catalyst concentration can contribute to sludge formation, increase total dissolved solids, increase COD and electrical conductivity [26]. In a photo-Fenton process, the high concentration of Fe^{2+} contributes to reducing the transmission of UV light [53]. Therefore, a homogeneous distribution of turbulent flow such as the one presented in Fig. 10 B contributes to an adequate release of Fe^{2+} throughout the reactor, without reducing the removal efficiency. Fig. 10 C shows the contour of Reynolds number of the flow into the reactor. The scale of color and values indicates that the flow maintains its turbulence in a range approximately of 5-6 and this guarantees the homogeneous distribution of flow pattern, avoiding zones with excessive or null turbulence.

4. Conclusions

The SCF process allows the removal of 100 mg L^{-1} of commercial PQ in an aqueous solution, with 2248 mg L^{-1} of H_2O_2 dosed in 28 min with a V_t/A_f ratio of 3.4:1, with a molar ratio H_2O_2:PQ of 170. An accumulated energy of 1554 kJ L^{-1} allowed the degradation of 100 % of PQ.

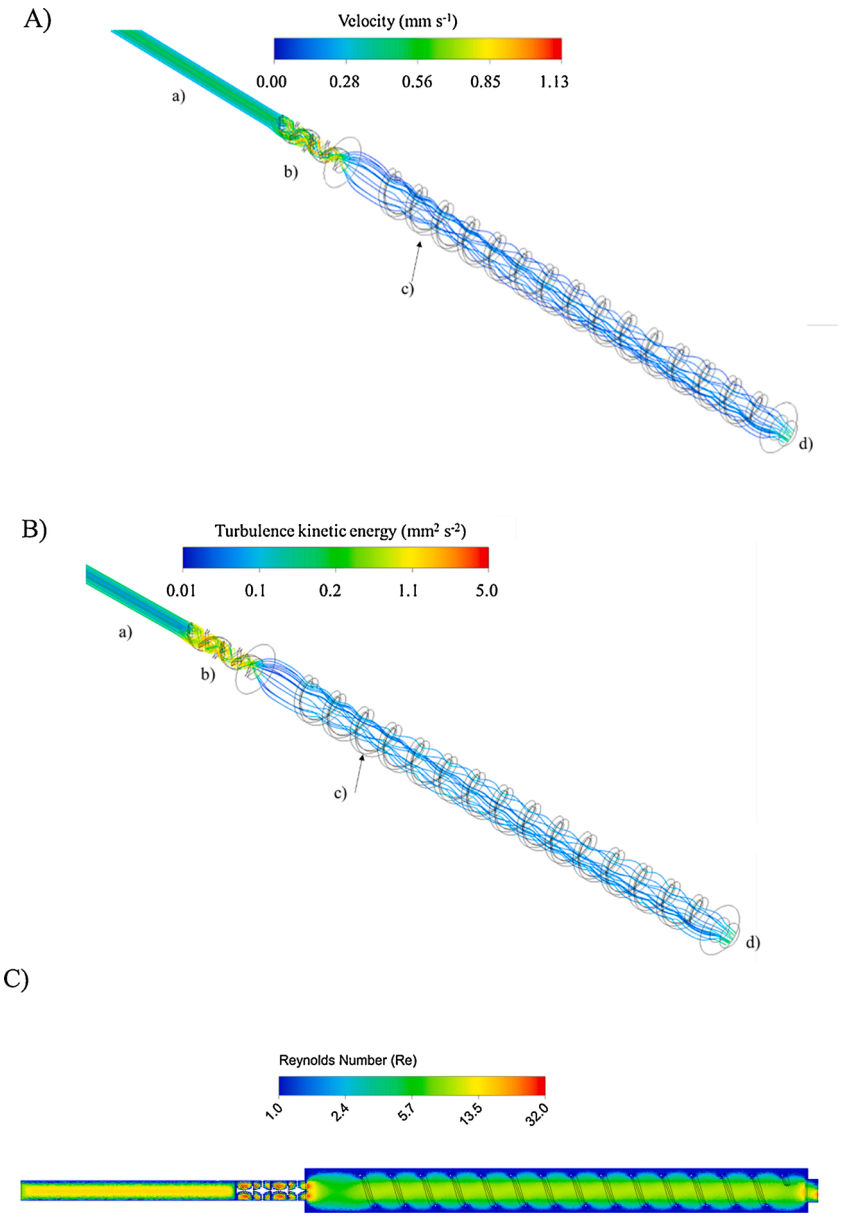

Fig. 10. Isometric view of the reactor. A) Streamlines of flow velocity in the reactor; B) Streamlines of flow for the turbulence kinetic energy: a) influent, b) static mixer, c) Fe filament, d) effluent; C) Contour of Reynolds number (lateral view).

When the energy was increased to 2021 kJ L^{-1}, a 94 % TOC removal was achieved, and a greater accumulated energy improved the mineralization. To remove the toxicity (Ec50), 700 mg L^{-1} of H_2O_2 was dosed and 1200 mg L^{-1} of H_2O_2 were necessary for a 90 % removal of PQ. It is possible that the adjuvants present in the commercial herbicide are responsible for increasing oxidant consumption. Photocorrosion is the main contributor mostly to the *in situ* release of Fe^{2+}, and the flow pattern contributes to a homogeneous concentration. Kinetic parameters indicate that the SCF process increases the rate of degradation of PQ, so a shorter time was necessary. Solar radiation favors the consumption of H_2O_2 and high radical formation of $HO^{\bullet}$. The SCF system uses sunlight to increase the reaction rate in the degradation of PQ, which reduces the treatment time and consumption of electrical energy. CFD indicated that operating speed and turbulence contributed to maintaining an adequate Fe^{2+} concentration.

Author statement

Luis A. Castillo-Suárez: Experimental design, statistical support, experimental tests, writing.

Ivonne Linares-Hernández: Conceptualization, investigation, validation, writing, original draft preparation.

Ruben Vasquez-Medrano: Reviewing, laboratory facilities and resources.

Jorge G. Ibanez: Supervision, reviewing and editing.

Fortunata Santoyo-Tepole: Methodology: HP analysis.

Boris Miguel López-Rebollar: CFD modelling.

Verónica Martínez-Miranda: Methodology: Infrared analysis and interpretation.

Declaration of Competing Interest

The authors report no declarations of interest.

Acknowledgments

This work was supported by the National Council for Science and Technology (CONACYT), Mexico through ID grants 212336, 710304, 441685 and 291277, and the economic support of the **Universidad Autónoma del Estado de México, ID project 6207-2020 CIB**. Use of facilities at Universidad Iberoamericana is gratefully acknowledged.

Appendix A. Supplementary data

Supplementary material related to this article can be found, in the online version, at doi:https://doi.org/10.1016/j.jphotochem.2021.113249.

References

[1] Z.E. Suntres, Exploring the potential benefit of natural product extracts in paraquat toxicity, Fitotherapy 131 (September) (2018) 160–167, https://doi.org/10.1016/j.fitote.2018.10.026.
[2] U.S. Environmental Protection Agency, Paraquat Dichloride [Online]. Available:, 2017 https://www.epa.gov/ingredients-used-pesticide-products/paraquat-dichloride.
[3] Priority Chemicals List, Environ. Prot. Auth., 2018. https://www.epa.govt.nz/public-consultations/decided/reassessment-of-paraquat/.
[4] X.H. Wang, C.L. Souders, Y.H. Zhao, C.J. Martyniuk, Paraquat affects mitochondrial bioenergetics, dopamine system expression, and locomotor activity in zebra fish (Danio rerio), Chemosphere 191 (2018) 106–117, https://doi.org/10.1016/j.chemosphere.2017.10.032.
[5] R.E. Ruiz-Nájera, J.A. Medina-Meléndez, J.C. Gómez-Castañeda, J.M. Sánchez-Yáñez, G. Gómez-Alfaro, O. Pinto-Molina, Study of the coffee production system (Coffea arabica L.) in the Frailesca region, Chiapas, CienciaUAT 10 (2) (2016) 33, https://doi.org/10.29059/cienciauat.v10i2.550.
[6] Syngenta, "Syngenta," Gramoxone [Online]. Available:, 2020 https://www.syngenta.com.mx/product/crop-protection/herbicide/gramoxoner.
[7] N. Thi Hue, T.P.M. Nguyen, H. Nam, N. Hoang Tung, Paraquat in surface water of some streams in Mai Chau Province, the Northern Vietnam: concentrations, profiles, and human risk assessments, J. Chem. 2018 (2018), https://doi.org/10.1155/2018/8521012.
[8] J. Ma, Y. Li, W. Li, X. Li, Hepatotoxicity of paraquat on common carp (Cyprinus carpio L.), Sci. Total Environ. 616–617 (2018) 889–898, https://doi.org/10.1016/j.scitotenv.2017.10.231.
[9] R. Saini, M.K. Mondal, P. Kumar, Fenton oxidation of pesticide methyl parathion in aqueous solution: kinetic study of the degradation, Environ. Prog. Sustain. Energy 36 (2) (2016) 1–8, doi: doi.org/10.1002/ep.12473.
[10] M.S.F. Santos, A. Alves, L.M. Madeira, Paraquat removal from water by oxidation with Fenton's reagent, Chem. Eng. J. 175 (1) (2011) 279–290, https://doi.org/10.1016/j.cej.2011.09.106.
[11] A.G. Trovó, O. Gomes, A.E.H. Machado, W.B. Neto, J.O. Silva, Degradation of the herbicide paraquat by photo-Fenton process: optimization by experimental design and toxicity assessment, J. Braz. Chem. Soc. 24 (1) (2013) 76–84, https://doi.org/10.1590/S0103-50532013000100011.
[12] R. Saini, M.K. Mondal, P. Kumar, Degradation of lignin in ionic liquid with HCl as catalyst, Environ. Prog. Sustain. Energy 35 (3) (2015) 809–814, https://doi.org/10.1002/ep.
[13] J.O. Trovó, A.G. Gomes Junior, Machado O, A.E.H. Borges Neto, Silva W, Degradation of the herbicide paraquat by photo-fenton process: optimization by experimental design and toxicity assessment, J. Braz. Chem. Soc. 24 (1) (2013) 76–84, https://doi.org/10.1590/S0103-50532013000100011.
[14] Y. Huang, H. Zhan, P. Bhatt, S. Chen, Paraquat degradation from contaminated environments: current achievements and perspectives, Front. Microbiol. 10 (August) (2019) 1–9, https://doi.org/10.3389/fmicb.2019.01754.
[15] C.B.D. Marien, Marie Le Pivert, Antonin Azaïsa Ignace Christian M'Bra, Patrick Drogui, Ahmad Dirany, Didier Robert, Kinetics and mechanism of Paraquat's degradation: UV-C photolysis vs UV-C photocatalysis with TiO_2 / SiC foams, J. Hazard. Mater. 370 (May) (2019) 164–171, https://doi.org/10.1016/j.jhazmat.2018.06.009.
[16] M.A.M. Cartaxo, C.M. Borges, M.I.S. Pereira, M.H. Mendonça, Electrochemical oxidation of paraquat in neutral medium, Electrochim. Acta 176 (2015) 1010–1018, https://doi.org/10.1016/j.electacta.2015.07.099.
[17] N.A. Badli, R. Ali, W. Azelee, W. Abu, L. Yuliati, Role of heterojunction $ZrTiO_4$ / $ZrTi_2O_6$ / TiO_2 photocatalyst towards the degradation of paraquat dichloride and optimization study by Box – Behnken design, Arab. J. Chem. (2017) 935–943, https://doi.org/10.1016/j.arabjc.2016.02.011.
[18] F. Zahedi, M. Behpour, S.M. Ghoreishi, H. Khalilian, Photocatalytic degradation of paraquat herbicide in the presence TiO_2 nanostructure thin films under visible and sun light irradiation using continuous flow photoreactor, Sol. Energy 120 (2015) 287–295, https://doi.org/10.1016/j.solener.2015.07.010.
[19] A. Dhaouadi, N. Adhoum, Degradation of paraquat herbicide by electrochemical advanced oxidation methods, J. Electroanal. Chem. Lausanne (Lausanne) 637 (1–2) (2009) 33–42, https://doi.org/10.1016/j.jelechem.2009.09.027.
[20] C. Annabi, et al., Degradation of enoxacin antibiotic by the electro-Fenton process: optimization, biodegradability improvement and degradation mechanism, J. Environ. Manage. 165 (2016) 96–105, https://doi.org/10.1016/j.jenvman.2015.09.018.
[21] D. Kanakaraju, B.D. Glass, M. Oelgemöller, Advanced oxidation process-mediated removal of pharmaceuticals from water: a review, J. Environ. Manage. 219 (2018) 189–207, https://doi.org/10.1016/j.jenvman.2018.04.103.
[22] M.S.F. Santos, A. Alves, L.M. Madeira, Paraquat removal from water by oxidation with Fenton's reagent, Chem. Eng. J. 175 (2011) 279–290, https://doi.org/10.1016/j.cej.2011.09.106.
[23] D. Spuhler, J. Antonio, Solar disinfection is an augmentable, in situ -generated photo-Fenton reaction – part 1: a review of the mechanisms and the fundamental aspects of the process, Applied Catal. B, Environ. 199 (2016) 199–223, https://doi.org/10.1016/j.apcatb.2016.06.009.
[24] A.I. Gomes, T.F.C.V. Silva, M.A. Duarte, R.A.R. Boaventura, V.J.P. Vilar, Cost-effective solar collector to promote photo-Fenton reactions: a case study on the treatment of urban mature leachate, J. Clean. Prod. 199 (2018) 369–382, doi: doi.org/10.1016/j.jclepro.2018.07.113.
[25] A.O. Roongkarn, P. Aphaiphak, J. Ananpattarachai, P. Kajitvichyanukul, Y. T. Hung, Heterogeneous Fenton and photo-Fenton reactions in paraquat removal using iron nanoparticles, Int. J. Environ. Waste Manag. 18 (1) (2016) 1–12, https://doi.org/10.1504/IJEWM.2016.080255.
[26] M.A. Behnajady, N. Modirshahla, F. Ghanbary, A kinetic model for the decolorization of C.I. Acid Yellow 23 by Fenton process, J. Hazard. Mater. 148 (1–2) (2007) 98–102, https://doi.org/10.1016/j.jhazmat.2007.02.003.
[27] Enric Brillas, Electro-fenton, UVA Photoelectro-Fenton and solar photoelectro-fenton treatments of organics in waters using a boron-doped diamond anode: a review, J. Mex. Chem. Soc. 58 (3) (2014) 239–255.
[28] K.C. Namkung, A.E. Burgess, D.H. Bremner, A fenton-like oxidation process using corrosion of iron metal sheet surfaces in the presence of hydrogen peroxide: a batch process study using model pollutants, Environ. Technol. 26 (3) (2005) 341–352, https://doi.org/10.1080/09593332608618564.
[29] K.C. Namkung, A.E. Burgess, D.H. Bremner, A fenton-like oxidation process using corrosion of Iron metal sheet surfaces in the presence of hydrogen peroxide: a batch process study using model pollutants, Environ. Technol. (October 2014) (2010) 37–41, https://doi.org/10.1080/09593332608618564.
[30] I.H. Yoon, et al., Kinetic study for phenol degradation by ZVI-assisted Fenton reaction and related iron corrosion investigated by X-ray absorption spectroscopy, Chemosphere 145 (2016) 409–415, doi: 0.1016/j.chemosphere.2015.11.108.
[31] M. Umar, H.A. Aziz, M.S. Yusoff, Trends in the use of Fenton, electro-Fenton and photo-Fenton for the treatment of landfill leachate, Waste Manag. 30 (11) (2010) 2113–2121, https://doi.org/10.1016/j.wasman.2010.07.003.
[32] A.G. Alcalá-Delgado, V. Lugo-Lugo, I. Linares-Hernández, V. Martínez-Miranda, R. M. Fuentes-Rivas, F. Ureña-Nuñez, Industrial wastewater treated by galvanic, galvanic Fenton, and hydrogen peroxide systems, J. Water Process Eng. 22 (October 2017) (2018) 1–12, https://doi.org/10.1016/j.jwpe.2018.01.001.
[33] L.A. Castillo-Suárez, V. Lugo-lugo, I. Linares-hernández, V. Martínez-miranda, M. Esparza-soto, M.D.L.Á. Mier-quiroga, Biodegradability index enhancement of landfill leachates using a Solar Galvanic-Fenton and Galvanic-Fenton system coupled to an anaerobic – aerobic bioreactor, Sol. Energy 188 (March) (2019) 989–1001, https://doi.org/10.1016/j.solener.2019.07.010.
[34] T.D. Burleigh, C. Ruhe, J. Forsyth, Photo-corrosion of different metals during long-term exposure to ultraviolet light, Corrosion 59 (9) (2003) 774–779, https://doi.org/10.5006/1.3277606.
[35] L. Song, Z. Chen, The role of UV illumination on the NaCl-induced atmospheric corrosion of Q235 carbon steel, Corros. Sci. 86 (2014) 318–325, https://doi.org/10.1016/j.corsci.2014.06.013.
[36] X. L, R.D. Sha Chen, Danlian Huang, Xu Piao, Wenjing Xue, Lei Lei, Min Cheng, Rongzhong Wang, Semiconductor-based photocatalysts for photocatalytic and photoelectrochemical water splitting: will we stop with photocorrosion? J. Mater. Chem. A Mater. Energy Sustain. 5 (2020) 2286–2322, https://doi.org/10.1039/C9TA12799B.
[37] Xiaofeng Ning, Lu Gongxuan, Photocorrosion inhibition of CdS-based catalysts for photocatalytic overall water splitting, Nanoscale 12 (3) (2020) 1213–1223, https://doi.org/10.1039/C9NR09183A.
[38] M. Zhou, Z. Guo, Z. Liu, FeOOH as hole transfer layer to retard the photocorrosion of Cu_2O for enhanced photoelectrochemical performance, " Appl. Catal. B Environ. 260 (2020) 118213, https://doi.org/10.1016/j.apcatb.2019.118213.
[39] J. Wang, Y. Zhang, X. Wang, W. Su, Simultaneous enhancements in photoactivity and anti-photocorrosion of Z-scheme $Mn_{0.25}Cd_{0.75}S/WO_3$ for solar water splitting, Appl. Catal. B Environ. 268 (2020) 118444, https://doi.org/10.1016/j.apcatb.2019.118444.
[40] J.E. Ramírez, et al., Swirling fluidization in an anoxic membrane bioreactor as an antifouling technique, J. Memb. Sci. 600 (January) (2020) 117856, https://doi.org/10.1016/j.memsci.2020.117856.
[41] S. Dash, S. Mohanty, B.K. Mishra, CFD modelling and simulation of an industrial scale continuous fluidized bed roaster, Adv. Powder Technol. 31 (2) (2020) 658–669, https://doi.org/10.1016/j.apt.2019.11.021.
[42] M.M. Gaber, Y.O. Fouad, H.A. Farag, G.H. Sedahmed, Intensification of the rate of diffusion controlled electrolytic oxidation of $FeSO_4$ by turbulence promoters in a stirred tank reactor in relation to wastewater treatment, Chem. Eng. Res. Des. 97 (2015) 100–108, https://doi.org/10.1016/j.cherd.2015.03.018.
[43] E. Quiroz-Pérez, C. Gutiérrez-Antonio, R. Vázquez-Román, Modelling of production processes for liquid biofuels through CFD: a review of conventional and intensified technologies, Chem. Eng. Process. - Process Intensif. 143 (August) (2019) 107629, https://doi.org/10.1016/j.cep.2019.107629.

[44] L.A. Castillo-Suárez, F. Bruno-severo, V. Lugo-lugo, Peroxicoagulation and solar peroxicoagulation for landfill leachate treatment using a Cu – Fe system, Water Air Soil Pollut. 229 (2018), https://doi.org/10.1007/s11270-018-4031-7.
[45] E.W. Rice, R.B. Baird, A.D. Eaton, Rice; Standard Methods for the Examination of Water and Wastewater, 23rd ed., American Public Health Association, American Water Works Association, Water Environment Federation, Washington DC, USA, 2017.
[46] P. Carbajal-Palacios, P. Balderas-Hernández, G. Roa-Morales, J.G. Ibanez, A greener UV and peroxide-based chemical oxygen demand test, Water Air Soil Pollut. 228 (8) (2017), https://doi.org/10.1007/s11270-017-3470-x.
[47] V.J.P. Vilar, et al., Biodegradability enhancement of a pesticide-containing bio-treated wastewater using a solar photo-Fenton treatment step followed by a biological oxidation process, Water Res. 46 (15) (2012) 4599–4613, https://doi.org/10.1016/j.watres.2012.06.038.
[48] S.B. Kolthoff IM, E.B. Sandell, E.J. Meehan, Quantitative Chemical Analysis, 4th ed. 1969, 4th ed., Macmillan, New York, 1969.
[49] U. Environmental Protection Agency, Protocols for Short Term Toxicity Screening of Hazardous Waste Sites [Online]. Available:, 1988 https://nepis.epa.gov.
[50] E.G. Fawaz, D.A. Salam, L. Kamareddine, Evaluation of copper toxicity using site specific algae and water chemistry: field validation of laboratory bioassays, Ecotoxicol. Environ. Saf. 155 (March 2018) (2018) 59–65, https://doi.org/10.1016/j.ecoenv.2018.02.054.
[51] T. Wang, Y. Zhou, S. Cao, J. Lu, Y. Zhou, Degradation of sulfanilamide by Fenton-like reaction and optimization using response surface methodology, Ecotoxicol. Environ. Saf. 172 (130) (2019) 334–340, https://doi.org/10.1016/j.ecoenv.2019.01.106.
[52] R.J. Dinis-Oliveira, Paula Guedes de Pinho, António C.ésar Silva Ferreira, Artur M.-S. Silva, Carlos Afonso, Maria de Lourdes Bastos, Fernando Remião, José Alberto Duarte, F.élix Carvalho, Reactivity of paraquat with sodium salicylate : formation of stable complexes, J. Toxicology 249 (2008) 130–139, https://doi.org/10.1016/j.tox.2008.04.014.
[53] I. Oller, S. Malato, J.A. Sánchez-pérez, Combination of Advanced Oxidation Processes and biological treatments for wastewater decontamination — a review, Sci. Total Environ. 409 (20) (2011) 4141–4166, https://doi.org/10.1016/j.scitotenv.2010.08.061.
[54] Sanae Kanno, Seishiro Hirano, Toshiji Mukai, Ayako Ro, Hideaki Kato, Mamiko Fukuta, Yasuhiro Aoki, Cellular uptake of paraquat determines subsequent toxicity including mitochondrial damage in lung epithelial cells, Leg. Med. 37 (November 2018) (2019) 7–14, https://doi.org/10.1016/j.legalmed.2018.11.008.
[55] X. Xu, Z. Cui, X. Wang, X. Wang, S. Zhang, Ecotoxicology and Environmental Safety Toxicological responses on cytochrome P450 and metabolic transferases in liver of gold fish (Carassius auratus) exposed to lead and paraquat, Ecotoxicol. Environ. Saf. 151 (December 2017) (2018) 161–169, https://doi.org/10.1016/j.ecoenv.2017.12.062.
[56] N.A. Badli, R. Ali, W.A. Wan Abu Bakar, L. Yuliati, Role of heterojunction $ZrTiO_4$/$ZrTi_2O_6$/TiO_2 photocatalyst towards the degradation of paraquat dichloride and optimization study by Box–behnken design, Arab. J. Chem. 10 (7) (2017) 935–943, https://doi.org/10.1016/j.arabjc.2016.02.011.
[57] A. Khudhair, M. Mahmudur, Environmental Technology & Innovation Kinetic of the degradation of sulfanilic acid azochromotrop (SPADNS) by Fenton process coupled with ultrasonic irradiation or L-cysteine acceleration, Environ. Technol. Innov. 15 (2019) 100380, https://doi.org/10.1016/j.eti.2019.100380.
[58] A. Brink, C.M. Sheridan, K.G. Harding, The Fenton oxidation of biologically treated paper and pulp mill effluents: A performance and kinetic study, Process Saf. Environ. Prot. 107 (2017) 206–215, https://doi.org/10.1016/j.psep.2017.02.011.
[59] Renato Grillo, Zaira Clemente, Jhones Luis de Oliveira, Estefânia Vangelie Ramos Campos, Victor C. Chalupe, Claudio M. Jonsson, Renata de Lima, Sanches Gabriel, S. Nishisaka Caroline, André H. Rosa, Kathleen Oehlke, Ralf Greiner, Leonardo F. Fraceto, Chitosan nanoparticles loaded the herbicide paraquat: the influence of the aquatic humic substances on the colloidal stability and toxicity, J. Hazard. Mater. 286 (2015) 562–572, https://doi.org/10.1016/j.jhazmat.2014.12.021.
[60] R. Mesnage, B. Bernay, G.E. Séralini, Ethoxylated adjuvants of glyphosate-based herbicides are active principles of human cell toxicity, Toxicology 313 (2–3) (2013) 122–128, https://doi.org/10.1016/j.tox.2012.09.006.
[61] R. Abrashev, E. Krumova, V. Dishliska, S. Engibarov, I. Abrashev, M. Angelova, Differential effect of paraquat and hydrogen peroxide on the oxidative stress response in Vibrio cholerae non O1 26 / 06, Biotechnol. Biotechnol. Equip. 2818 (2014), https://doi.org/10.5504/BBEQ.2011.0118.
[62] F.S.-T. Saúl González-Cuna, Juvencio Galíndez-Mayer, Ruiz-Ordaz Nora, Selvasankar Murugesan, Alberto Piña-Escobedo, Jaime García-Mena, Emanuel Lima-Martínez, Aerobic biofilm reactor for treating a commercial formulation of the herbicides 2, 4-D and dicamba: biodegradation kinetics and bio film bacterial diversity, Int. Biodeterior. Biodegradation 107 (2016) 123–131, https://doi.org/10.1016/j.ibiod.2015.11.014.
[63] E.A. Lock, M.F. Wilks, "Paraquat," Hayes' Handb. Pestic. Toxicol., no. 1958, Elsevier Inc, San Diego C.A, 2010, pp. 1771–1827, https://doi.org/10.1016/B978-0-12-374367-1.00083-5.
[64] S.S. Lele, J.B. Joshi, Modelling of air-lift fluidized bed: Optimization of mass transfer with respect to design and operational parameters, Chem. Eng. J. 49 (2) (1992) 89–105, https://doi.org/10.1016/0300-9467(92)80043-A.